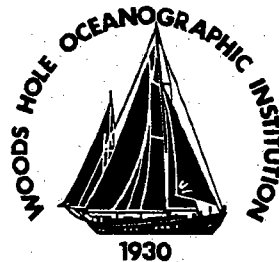
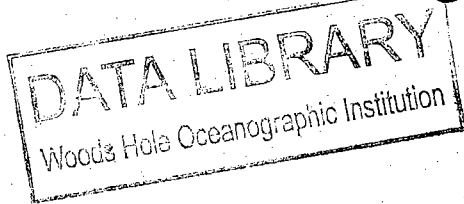


WHOI-00-13

*Copy 2*

**Woods Hole  
Oceanographic  
Institution**



---

**An Improved Long-Wave Radiometer**

by

Steven P. Anderson  
and  
Richard E. Payne

December 2000

**Technical Report**

Funding was provided by the Cecil H. and Ida M. Green Technology Innovations Awards Program and the National Science Foundation, Grant OCE98-18470.

Approved for public release; distribution unlimited.

---



WHOI-00-13

**An Improved Long-Wave Radiometer**

by

Steven P. Anderson  
and  
Richard E. Payne

Woods Hole Oceanographic Institution  
Woods Hole, Massachusetts 02543

December 2000

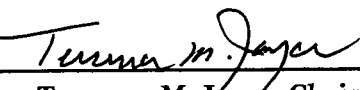
**Technical Report**

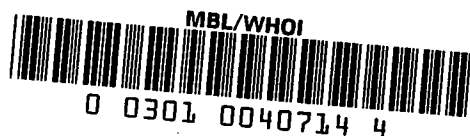
Funding was provided by the Cecil H. and Ida M. Green Technology Innovations Awards Program and the National Science Foundation, Grant OCE98-18470.

Reproduction in whole or in part is permitted for any purpose of the United States Government. This report should be cited as Woods Hole Oceanog. Inst. Tech. Rept., WHOI-00-13

Approved for public release; distribution unlimited.

**Approved for Distribution:**

  
\_\_\_\_\_  
Terrence M. Joyce, Chair  
Department of Physical Oceanography



This page intentionally left blank.

# Contents

<b>Abstract</b>	<b>5</b>
<b>1 Introduction</b>	<b>5</b>
<b>2 Background</b>	<b>7</b>
2.1 Pyrgeometer theory . . . . .	8
2.2 The Eppley PIR . . . . .	10
2.3 Calibration coefficients . . . . .	11
2.4 Thermal gradients and other sources of measurement error . . . . .	14
<b>3 Rethinking the pyrgeometer design</b>	<b>16</b>
3.1 Replacing the thermopile . . . . .	16
3.2 The dome heating correction . . . . .	19
<b>4 Demonstration of concept</b>	<b>23</b>
4.1 The prototype . . . . .	24
4.2 Calibration . . . . .	24
4.3 Field intercomparison . . . . .	28
<b>5 Conclusions</b>	<b>34</b>
<b>Appendix</b>	<b>35</b>
Clark et al. formulation . . . . .	35
Cloud cover estimation . . . . .	35
<b>Acknowledgments</b>	<b>37</b>
<b>References</b>	<b>38</b>

This page intentionally left blank.

## Abstract

This report describes the development of an improved long-wave radiometer (pyrgeometer) for deployment on ships and buoys. Standard pyrgeometers use a thermopile to measure the temperature gradient between the receiver surface and the instrument case, and thus infer the receiver temperature and incident radiation. The key design change employed in the new radiometer is to remove the thermopile and replace it with a small, glass-encapsulated thermistor to measure the receiver temperature directly. To prove the concept, a prototype radiometer was built and calibrated. It was then deployed outside for a period of a week on the roof of the Clark Laboratory (Quissett Campus, Woods Hole Oceanographic Institution) to demonstrate the feasibility of the new concept. Data from the prototype were compared to those from a pair of standard radiometers. The intercomparison shows that the prototype performed surprisingly well. It was able to capture all the variability observed by the standards with only a small bias. The next step in the design process, which has been funded by the National Science Foundation, is to build a rugged version of the prototype that can be deployed in the field.

## 1 Introduction

Recent climate research programs are demanding an increased accuracy of air–sea flux estimates. The surface long-wave (infrared) radiation fluxes have not commonly been measured at sea, and improvement of the long-wave radiation instrumentation is needed to meet these demands. Improved meteorological measurements and aerodynamic bulk formulae have brought net errors in short-wave radiation and latent and sensible heat fluxes down to approximately  $10 \text{ W m}^{-2}$ . Conservative error estimates for typical long-wave radiation flux measurements are  $10 \text{ W m}^{-2}$  at night and  $40 \text{ W m}^{-2}$  during the day. Thus the long-wave radiation is the source of the largest uncertainty in air–sea surface energy budgets.

Long-wave radiation is a difficult measurement to make from a ship, since the ship itself is often a source of infrared radiation and internal heating effects in the radiometers make the instruments nearly useless unless care is taken to shade the instrument from direct sunlight. The Eppley Precision Infrared Radiometer (PIR) has been the standard in the atmospheric

research community for over 20 years and is often deployed on land and aircraft. Surprisingly, few users fully understand the instrument or are aware of (or just accept) its limitations. And even fewer have access to calibration facilities for these instruments. The Woods Hole Oceanographic Institution now has one of only a handful of calibration facilities in the world (Payne and Anderson, 1999). The expertise gained in setting up this facility has placed us in a unique position to begin design improvements.

In this report, we describe an effort to develop an improved long-wave radiometer (pyrgeometer), for deployment on ships and buoys, using our improved understanding of the instrument and modern measurement techniques. The new design overcomes some of the limitations of the currently available instrumentation, and will lead to a reduction of the errors in measuring surface long-wave radiation.

In our redesign of the pyrgeometer, we endeavored to develop an instrument that met the following criteria:

- is easily calibrated and the calibrations remain stable even under unfavorable conditions;
- has few components and is easily fabricated;
- is not significantly affected by short-wave radiative heating effects of the radiometer body; and
- is rugged and reliable enough to withstand a 12-month deployment on a surface buoy.

Standard radiometers, like the Eppley PIR, employ a thermopile to measure the receiver surface temperature. This technique was required to increase the instrument's sensitivity. Eliminating the thermopile is a revolutionary idea, and its good sense is the major finding presented here. The thermopile has been in use for decades and the research community has been in a bit of rut. We found no need to use a thermopile in the instrument since the required sensitivity could be achieved with inexpensive glass-encapsulated thermistors. Removing the thermopile will reduce costs of fabrication and improve the measurement capability. We envision the community embracing this technique in the coming years.

A review of theory of pyrgeometer operation is presented in Section 2. In Section 3, we discuss our considerations for redesigning the Eppley PIR. Our experiences in designing



and fabricating a prototype and validating the new measurement technique are in Section 4. We successfully demonstrate that the prototype not only works but performs remarkably well. The Appendix includes some information on using empirical formulae for estimating long-wave radiation at the ocean surface.

## 2 Background

The net long-wave flux at the sea surface is the difference between the downward ( $LW \downarrow$ ) and upward radiation ( $LW \uparrow$ )

$$LW \uparrow \downarrow = LW \uparrow - LW \downarrow \quad (1)$$

$LW \uparrow \downarrow$  is a function of sea surface skin temperature  $T_{s^*}$ , sea surface emissivity,  $\epsilon$ , and the profiles of temperature and humidity in the lower atmosphere. The upward flux is given by

$$LW \uparrow = \epsilon \sigma T_{s^*}^4 \quad (2)$$

where  $\sigma$  is the Stefan-Boltzmann constant. Empirical formulae assume that in a cloud-free regime, the net long-wave radiation can be described as a function of the sea surface temperature,  $T_s$ , the air temperature,  $T_a$ , and the near-surface water vapor pressure,  $e_a$ . These formulae are effective at predicting the net long-wave radiation in clear sky. The difficulty is in parameterizing the effect of cloud cover using observable quantities. Cloud cover observations are taken by shipboard observers who are trained to estimate cloud base height and cover by eye. An alternative approach is to use measured incoming solar insolation and compare it with the theoretical clear sky values to estimate the cloud cover. This method, however, does not yield any information about cloud height. (See Fung et al., 1984, for a review of empirical formula.)

The preferred method of estimating net long-wave flux is a “hybrid measurement system” where the incoming long-wave radiation at the sea surface is measured and the outgoing long-wave radiation is estimated from sea surface temperature measurements. The formulation is

$$\begin{aligned} LW \uparrow \downarrow (0) &= LW \uparrow (0) - LW \downarrow (0) \\ &= \epsilon_{ss} \sigma T_{ss}^4 - (1 - \epsilon_{ss}) LW \downarrow (0) \end{aligned} \quad (3)$$

where  $\epsilon_{ss}$  is the sea surface emissivity ( $0.985 \pm 0.010$ ),  $T_{ss}$  is the sea surface temperature, and  $LW\downarrow(0)$  is the measured incoming long-wave radiation flux at the sea surface.

## 2.1 Pyrgeometer theory

In the ideal pyrgeometer, the downwelling radiation is estimated from the balance of absorbed radiation to emitted radiation from a surface. The heat budget for the surface is simply

$$\begin{aligned} H &= R_{\text{net}} \\ &= \alpha R\downarrow - \epsilon_0 \sigma T_s^4 \end{aligned} \quad (4)$$

where  $H$  is the heat gain to the surface from conduction or convection,  $R_{\text{net}}$  is the net radiation on the surface,  $T_s$  is the receiver temperature,  $R\downarrow$  is the incoming radiation from the environment,  $\alpha$  is the absorption coefficient of the surface ( $\alpha = \epsilon_0 = 1$  for a black body), and  $\epsilon_0$  is the surface emittance. In the ideal case,  $H$  is zero,  $T_s$  is measured, then the  $R\downarrow$  is calculated. In practice, no instrument can be built with this simple heat budget.

The first difficulty is that the receiving surface cannot be supported and  $T_s$  cannot be measured without creating a path for conductive heat loss. Thus there must be a case that supports the receiving surface and dome. If the heat loss to the case is only conduction, it can be written as

$$k(T_s - T_c) \quad (5)$$

where  $k$  is a heat transfer coefficient for the conductive heat loss between the surface and the case. (Note that this term should be as small as possible. External heating of the case may lead to thermal gradients along the path between  $T_s$  and  $T_c$  which are not just a simple function of the conduction of heat away from the receiving surface. This would lead to a poor estimate of the conductive heat loss from the surface to the case.) Adding in this term, the heat budget then becomes

$$k(T_s - T_c) = \alpha R\downarrow - \epsilon \sigma T_s^4 \quad (6)$$

Note that  $k$  will depend on materials and geometry of the case.

The second difficulty is designing a filter that restricts transmitted radiation to long-wave only. This is usually implemented with a hemispherical silicon dome with an interference filter coating on the inside. The dome transmittance must be a function of wavelength. It will be assumed here that it has one value in the short-wave band and another in the long-wave band. The transmitted radiation is

$$R\downarrow = \tau_d^{SW} SW\downarrow + \tau_d^{LW} LW\downarrow \quad (7)$$

where  $SW\downarrow$  and  $LW\downarrow$  are incident short-wave and long-wave radiation fluxes and  $\tau_d^{SW}$  and  $\tau_d^{LW}$  are the transmittance in each band. The dome unfortunately also acts a source and reflector of radiation. Thus the net radiation of the receiver surface is

$$R_{\text{net}} = R\downarrow + R\uparrow \quad (8)$$

where

$$R\uparrow = \epsilon_0 \sigma T_s^4 + (1 - \epsilon_0) R\downarrow \quad (9)$$

and

$$R\downarrow = \tau_d^{SW} SW\downarrow + \tau_d^{LW} LW\downarrow + \rho R\uparrow + \epsilon \sigma T_d^4 \quad (10)$$

where  $\rho$  and  $\epsilon$  are the long-wave reflectance and emittance of the dome and  $T_d$  is the dome temperature. Note that in the above equation, it is assumed that there are no short-wave emissions from either the dome or the receiving surface. Taking note of the fact that  $(1 - \rho) = \epsilon + \tau$ , we can solve for  $LW\downarrow$  directly

$$LW\downarrow = \underbrace{\sigma T_s^4}_{\text{(I)}} + \underbrace{\frac{[1 - \rho(1 - \epsilon_0)]}{\tau_d^{LW} \epsilon_0} k(T_s - T_c)}_{\text{(II)}} + \underbrace{\frac{\epsilon \sigma}{\tau_d^{LW}} (T_s^4 - T_d^4)}_{\text{(III)}} - \underbrace{\frac{\tau_d^{SW}}{\tau_d^{SW}} SW\downarrow}_{\text{(IV)}} \quad (11)$$

The four terms are (I) the black body emission from the surface, (II) the heat lost due to conduction to the case, (III) the radiative heat flux from the dome, and (IV) the short-wave leakage through the dome. This is the same as Equation 7 of Fairall et al. (1998) except for the inclusion of the short-wave transmittance. The  $LW\downarrow$  could theoretically be estimated from measured  $SW\downarrow$ ,  $T_s$ ,  $T_c$ , and  $T_d$ .

## 2.2 The Eppley PIR

The standard pyrgeometer, designed about 30 years ago, is the Eppley Precision Infrared Radiometer (PIR). This instrument employs a silicon hemisphere dome which provides a nominal passband of approximately 4–50  $\mu\text{m}$ , isolating terrestrial long-wave radiation from the solar short-wave radiation. The radiation is sensed using a non-wavelength selective thermopile detector located beneath the dome and a thermistor located in the case. The thermopile consists of 60 thermocouples in series to increase the sensitivity. The thermopile measures a temperature difference rather than an absolute temperature. The hot junction of the thermopile forms the receiving surface, and the cold junction is in thermal contact with the case. The voltage output of the thermopile is

$$s_0^{-1}V_{\text{out}} = (T_s - T_c) = \Delta T \quad (12)$$

where  $s_0$  is the thermopile sensitivity. One of the thermistors,  $T_c$ , is placed as close as possible to the thermopile cold junction. Another thermistor,  $T_d$ , is attached to the inside of the dome. Substituting these temperatures into the above equation, the incoming long-wave is

$$LW\downarrow = \underbrace{\sigma(T_c + \Delta T)^4}_{\text{(I)}} + \underbrace{\frac{[1 - \rho(1 - \epsilon_0)]}{\tau_d^{LW} \epsilon_0}}_{\text{(II)}} k\Delta T + \underbrace{\frac{\epsilon\sigma}{\tau_d^{LW}} [(T_c + \Delta T)^4 - T_d^4]}_{\text{(III)}} - \underbrace{\frac{\tau_d^{SW}}{\tau_d^{LW}} SW\downarrow}_{\text{(IV)}} \quad (13)$$

To make this equation look like the formulation by Albrecht and Cox (1977)

$$L = E(c_1 + c_2 T_c^3) + \epsilon_0 \sigma T_c^4 - k\sigma(T_d^4 - T_c^4) \quad (14)$$

the following assumptions must be made:

$$\begin{aligned} \tau_d^{SW} &= 0 \\ \Delta T &\ll T_c \text{ so that } (\Delta T + T_c)^4 \approx T_c^4 + 4T_c^3 \Delta T \end{aligned} \quad (15)$$

Then the downwelling long-wave equation reduces to

$$LW\downarrow = \sigma T_c^4 + s_e^{-1}V_{\text{out}} \left\{ k \frac{[1 - \rho(1 - \epsilon_0)]}{\tau_d^{LW} \epsilon_0} + 4 \left( 1 + \frac{\epsilon_d}{\tau_d^{LW}} \right) \sigma T_c^3 \right\} + \frac{\epsilon_d}{\tau_d^{LW}} \sigma (T_c^{*4} - T_d^{*4}) \quad (16)$$

[This formulation is different from that of Alados-Arboledas et al. (1988, Eq. 2). They have a term  $T_c^3$  term which is not multiplied by  $\Delta T$ . It is not clear where this term could come from since it must be derived from the Taylor series expansion.]

In the standard Eppley pyrgeometer configuration, the contribution of the last term in Eq. 16 is ignored. The Eppley sensor uses a compensation circuit to combine the thermopile output voltage, the case thermistor resistance, and a reference battery voltage. The voltage out of the unit is directly proportional to  $LW \downarrow$  (see Fig. 1). This configuration was used in both the vector-averaging wind recorders (VAWR) and improved meteorological (IMET) PIRs deployed on the WHOI surface mooring during TOGA COARE (Tropical Ocean Global Atmosphere Coupled Ocean-Atmosphere Response Experiment). When the units are calibrated, there is a potentiometer that should be adjusted to tune the compensating circuit for zero error at typical deployment temperatures. We have not tested this but it is unlikely that this was done. (For full description of the errors from the compensation circuit, see Olivieri, 1991.)

The current version of the IMET PIR measures the three outputs, thermopile voltage, dome and case thermistor resistances, separately, and computes temperatures and total long-wave irradiance by Eq. 16. Also, the IMET PIR has an all-aluminum case with no radiation shield whereas the stock Eppley PIR is constructed with brass, stainless steel and aluminum with a radiation shield. See Payne and Anderson (1999) for details. At the time of the initial PIR design, Eppley had been building pyranometers based on a clever use of a thermopile for some time. It probably was not feasible, given the thermistor technology of the time, to design a pyrgeometer which used thermistors exclusively. Use of the thermopile was a reasonable choice.

### 2.3 Calibration coefficients

Equation (11) can be simply rewritten using a coefficient for each of terms II, III and IV such that

$$LW \downarrow = \underbrace{\sigma T_s^4}_{(I)} + \underbrace{A(T_s - T_c)}_{(II)} + \underbrace{B(T_s^4 - T_d^4)}_{(III)} - \underbrace{C SW \downarrow}_{(IV)} \quad (17)$$

# PRECISION INFRARED RADIOMETER - MODEL PIR (PYRGEOMETER)

## INTERNAL WIRING

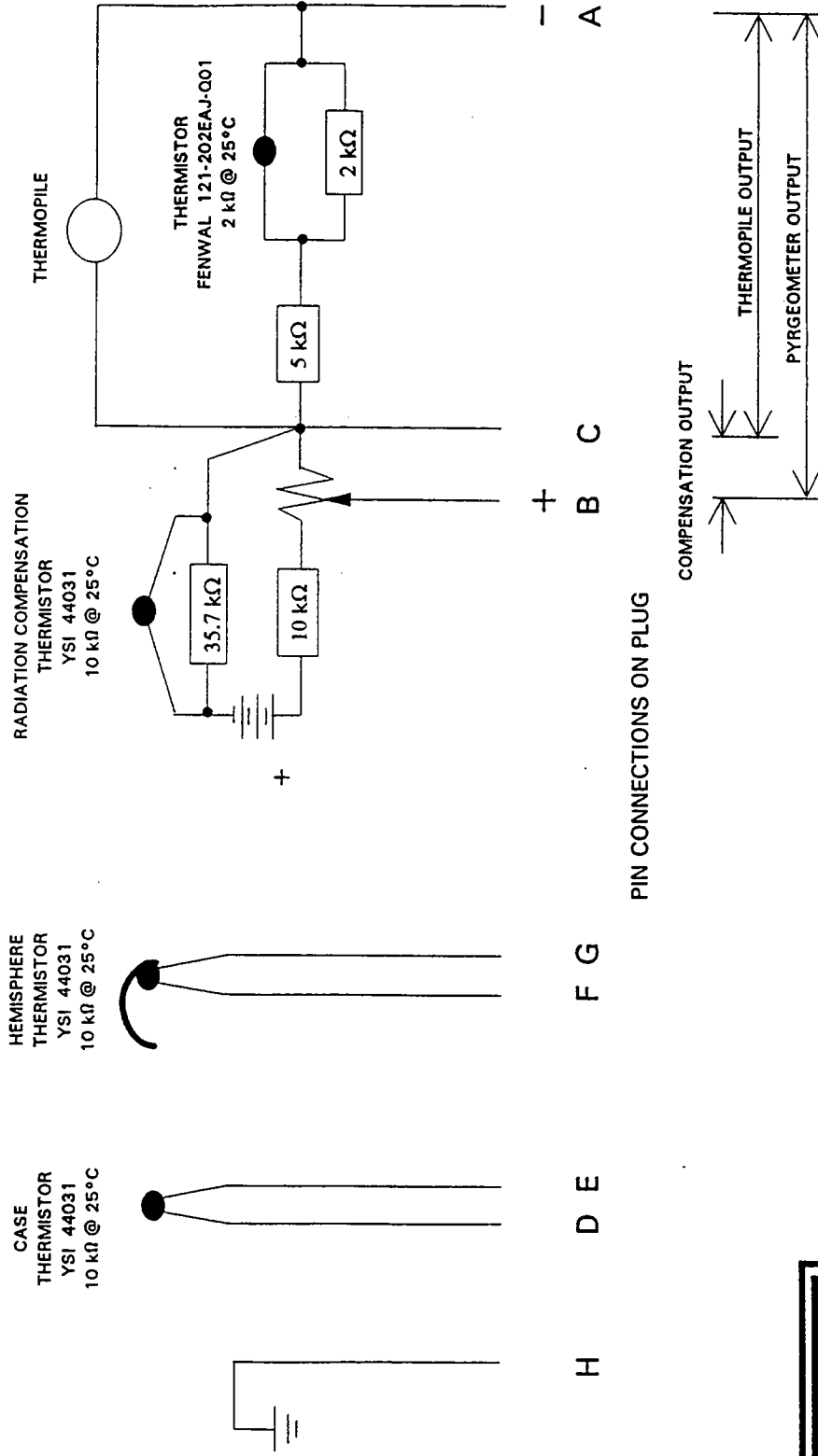


Figure 1: Eppley Precision Infrared Pyrometer circuit schematic.



**Table 1**  
**Suggested values for Eppley PIR radiative terms**

		Dickey et al. (1994)	Olivieri (1991)
long-wave transmissivity of the dome	$\tau_d$	$0.27 \pm 0.01$	0.34
short-wave transmissivity of the dome	$\tau_d^{SW}$	$0.0098 \pm 0.005$	0.003
long-wave reflectivity of the dome	$\rho_d$	0.4	—
short-wave reflectivity of the dome	$\rho_d^{SW}$	0.99	—
long-wave emissivity of the dome	$\epsilon_d$	$0.3 \pm 0.1$	—
short-wave emissivity of the dome	$\epsilon^{LW}, \epsilon_d^{SW}$	0.0	—
long-wave emissivity of the receiving surface	$\epsilon$	$0.91 \pm 0.01$	0.985
reflectivity of the receiving surface	$\rho^{LW}, \rho^{SW}$	$0.02 \pm 0.01$	—

where  $A$ ,  $B$  and  $C$  are coefficients determined by calibration. The coefficients  $A$  and  $B$  can be determined directly with a black body cavity using the procedure described by Payne and Anderson (1999) who do not evaluate  $C$ . The  $B$  term is directly related to the Albrecht and Cox (1977)  $k$  term. The  $A$  coefficient, however, is not directly relatable to the  $c_1$  and  $c_2$  terms for Albrecht and Cox (1977, their Eq. 15). Note that, because of the difficulties of applying the interference coating to the dome interior, the long-wave transmittance and emissivity and the short-wave of the dome vary from one dome to another leading to a variation in values of  $B$ .

Dickey et al. (1994) suggest values of all the radiative constants (See Table 1). They employ the PIR equation written as

$$LW\downarrow = \underbrace{0.91\sigma T_c^{*4}}_{(I)} + \underbrace{s_e^{-1}V_{out}(0.976B + 8.08\sigma T_c^{*3})}_{(II)} + \underbrace{1.11(T_d^4 - T_c^4)}_{(III)} + \underbrace{0.0367SW\downarrow}_{(IV)} \quad (18)$$

The value of  $B$  is determined from calibration, and Dickey et al. do not attempt to propose a value for it. Note that the coefficient of 0.91 is compared with 1.0 multiplying term (I) in Eq. 17. Using this coefficient, a value of  $T_c = 300^\circ\text{K}$  corresponds to a difference in  $LW\downarrow$  of  $41 \text{ W m}^{-2}$ .

Dickey et al. arrive at short-wave transmittance by assuming that most of the solar effect seen by Alados-Arboledas et al. (1988) is from solar radiation being transmitted through the dome. Olivieri (1991) proposed a much smaller short-wave transmittance. He assumes the transmission of the silicon dome is negligible below  $2.5\mu\text{m}$ . Since solar irradiance is negligible above  $5\mu\text{m}$ , one only needs to consider a small band of short-wave radiation. Olivieri's estimates would lead to noon time errors in  $LW\downarrow$  of only  $1.2\text{ W m}^{-2}$  for a  $SW\downarrow$  of  $400\text{ W m}^{-2}$  as opposed to  $14.78\text{ W m}^{-2}$  from Dickey et al. Olivieri also suggests a much larger long-wave transmittance of  $\tau_d = 0.34$ .

Olivieri proposes that the major solar error signal is from overheating of the dome. This is consistent with Albrecht and Cox (1977) who present observations of the heating of the dome and its effect on measured downwelling long-wave radiation. They find that this error is nearly a direct function of observed short-wave radiation. They suggest an empirical correction for direct solar heating of the pyrgeometer dome using observed  $SW\downarrow$ .

$$k\sigma(T_c^{*4} - T_d^{*4}) = a SW\downarrow + b \frac{\Delta SW\downarrow}{\Delta t} \quad (19)$$

This formulation uses the time-lagged observed short-wave radiation to account for the thermal mass of the pyrgeometer. This may be important for the fast response observations they took from an aircraft, however, this term will be small in the moored observation time series. They suggest a solar heating coefficient,  $a$ , of 0.0311 ( $b = 0.0666$ ) which is nearly the same as Dickey et al. It is important to note that this coefficient is proportional to their  $k$ . It appears that the formulation of Dickey et al. is flawed. Their formulation should either have the dome temperature correction term or the empirical correction using the observed  $SW\downarrow$ , but not both. It appears that the short-wave transmittance is indeed small and can be largely ignored while the dome heating term must be accounted for in long-wave calculations.

## 2.4 Thermal gradients and other sources of measurement error

Thermal gradients within the pyrgeometer are another source of error. This is not accounted for in the theory nor given much attention. Foot (1986) has identified thermal gradients in the case and dome. Measurement errors will result since the case temperature may not be representative of the cold junction side of the thermopile. In addition, thermal gradients across the dome mean the dome thermistor does not accurately represent the



**Table 2**  
**Summary of uncertainty for Eppley PIR**  
**long-wave measurements**

		term			
		(I)	(II)	(III)	total (W m <sup>-2</sup> )
$T_c$	$\pm 0.100^\circ\text{K}$	$\pm 0.6$		$\pm 1.3$	$\pm 1.9$
$\Delta T$	$\pm 0.005^\circ\text{K}$	$\pm 0.03$	$\pm 2.0$	$\pm 0.1$	$\pm 2.0$
$T_d$	$\pm 0.200^\circ\text{K}$			$\pm 2.6$	$\pm 2.6$
$A$	4 %		$\pm 3.1$		$\pm 3.1$
$B$	4 %			$\pm 0.8$	$\pm 0.8$
<b>Total uncertainty</b>		<b><math>\pm 0.6</math></b>	<b><math>\pm 3.7</math></b>	<b><math>\pm 3.0</math></b>	<b><math>\pm 5.0</math></b>

average temperature of the dome (Philipona et al., 1995). There have been attempts to measure the dome temperature at three different locations around the dome simultaneously, but there are no documented attempts at measuring the case temperature gradients directly.

Another source of error is the thermistors themselves. Payne and Anderson (1999) report that the PIR thermistors must be calibrated since some depart significantly from the manufacturer's specification, particularly the dome thermistors. This is not typically done however. There is no technique available for calibrating the thermopile sensitivity directly, and its small output voltages place a very low noise and high accuracy demand on the amplifier and A/D sampling electronics. There also remains some uncertainty in the calibration coefficients.

A summary of the uncertainties in the Eppley PIR measurements is given in Table 2. These assume that  $T_c = 300^\circ\text{K}$ ,  $T_d = 301^\circ\text{K}$ ,  $\Delta T = -0.2^\circ\text{K}$ ,  $A = 390$ , and  $B = 2.8$ . It appears that for times longer than a week, the PIR accuracy may approach  $\pm 6 \text{ W m}^{-2}$  as validated by intercomparisons (Fairall et al., 1998; Payne and Anderson, 1999). However, the instantaneous accuracy can be much worse, close to  $\pm 30 \text{ W m}^{-2}$ .

### 3 Rethinking the pyrgeometer design

The Eppley PIR uses a thermopile to measure the receiver surface temperature. This technique was required to increase the instrument sensitivity, however, it makes the instrument susceptible to thermal gradients across the case and there is significant conductive heat loss from the receiving surface to the case through the thermopile. In addition, the size of the hot junction accounts for only 17% of the area below the dome, which results in large amounts of emitted and reflected radiation from the case being absorbed by the detector. Finally, the instrument cases are made of brass and stainless steel which have poor thermal characteristics and are susceptible to corrosion in the marine environment.

Here, we reexamine the PIR and seek to improve on the design in three specific ways. First, new glass-encapsulated thermistors and associated electronics allow for the direct measurement of the detector temperature with the required sensitivity and would replace the thermopile. This allows for better isolation of the detector from the case and for easier calibration. Secondly, the case would be constructed to minimize the conductive heat loss of the receiver to the case and reduce temperature gradients in the case. Thirdly, the size of the detector would be enlarged to nearly 100% of the available area under the dome which would increase the detector sensitivity.

#### 3.1 Replacing the thermopile

The thermopile has been a tool in radiation measurement for decades. These devices are expensive to fabricate, and an absolute calibration is usually not available. But is the precision of temperature differences the thermopile provides really needed in the pyrgeometer? Can we eliminate the thermopile altogether and measure the temperature of the receiver surface directly using a glass-encapsulated thermistor and still achieve measurement uncertainties of  $5 \text{ W m}^{-2}$  or better? This would allow for a cheaper-to-build and easier-to-calibrate pyrgeometer.

With a glass-encapsulated thermistor, we conservatively can measure temperatures to  $\pm 0.010^\circ\text{K}$  and often much better. Using Eq. 17, a  $0.010^\circ\text{K}$  error in  $T_s$  translates into a (I)  $0.1 \text{ W m}^{-2}$  error in the black body emittance term, (II)  $3.9 \text{ W m}^{-2}$  error in the conductive

heat loss term, and (III)  $0.1 \text{ W m}^{-2}$  error in the dome heating term (assuming  $A = 390$  and  $B = 2.8$ ). The only term in the pyrgeometer equation that requires the high sensitivity is the conductive heat loss term. This result was not intuitive to us.

If the pyrgeometer can be redesigned such as to reduce the conductive heat loss term (III), the sensitivity achieved with the thermopile is not needed. This would require increasing the dome transmissivity in the long-wave band, increasing the emissivity ( $\epsilon_0$ ) of the receiver surface, or decreasing the conductive heat loss coefficient,  $k$ , to the case. The emissivity of Eppley-Parsons black lacquer, used on the receiver of the PIR, is 0.985, so there is not much room for improvement. The transmissivity of the dome in the long-wave is approximately 0.35. It is unlikely that the dome long-wave transmissivity could be increased without increasing the short-wave transmissivity, which would cause other problems. If it could be increased, it would also reduce the dome reflectance and emittance terms and reduce the dome heating errors. However, we did not explore this option since it is beyond our expertise at this time. The only domes available to us are those made by Eppley.

We can, however, attempt to reduce the conduction of heat from the receiver to the case. In fact, doing away with the thermopile gives us the flexibility to do this. In the thermopile, the thermocouple wire is wound around an aluminum T-shaped support (see Fig. 2), and the cold junction of the thermopile must be in good thermal contact with the case through the arms of the T. This assures a good conductive heat path. Without the thermopile, we are free to insulate the receiver from the case, effectively reducing the coefficient  $k$ . What we found in our subsequent testing is that this term can, indeed, be readily reduced by nearly a factor of 4. In our prototype, discussed in the next section, the coefficient  $A$  is 110 while for most Eppley PIRs this number is near 400.

We note here, and again later, that although reducing the heat loss to the case is important, just as important is still being able to accurately estimate term (II) in the instrument since there will always be some conduction to the case. We found that using case materials with low heat conductivity supported large temperature gradients in the case and that no meaningful  $T_c$  measurement could be made to effectively quantify term (II).

The reduction of the need for high sensitivity is not the only advantage to replacing the thermopile. By reducing the magnitude of the heat loss term (III), we reduce the importance

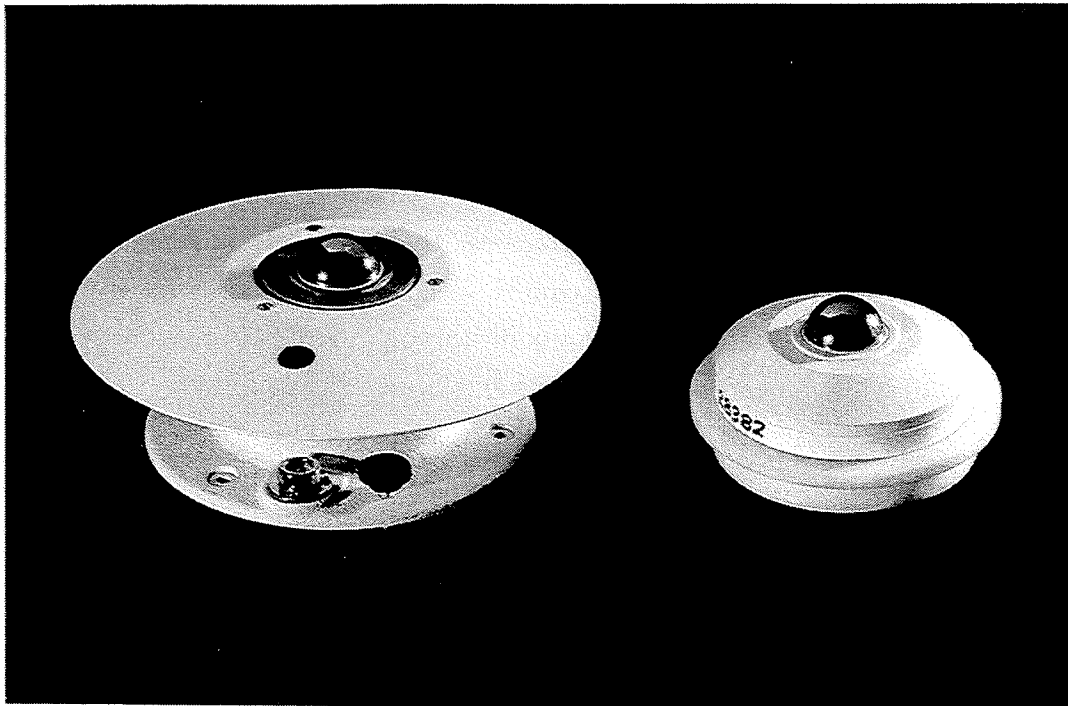
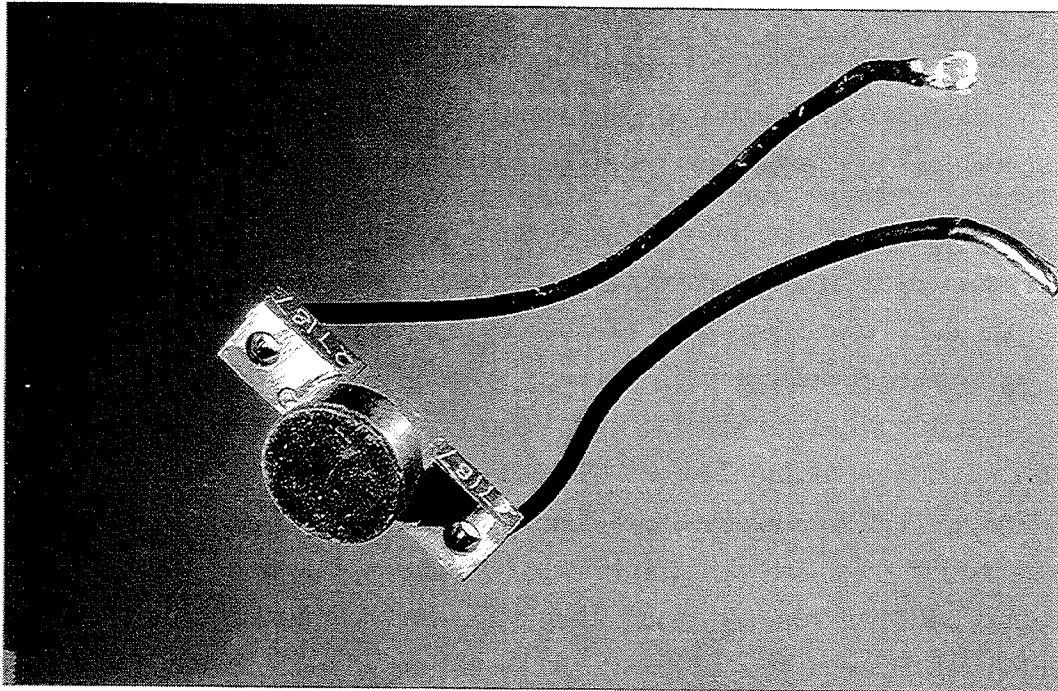


Figure 2: Upper panel: Photograph of thermopile from Eppley PIR. Lower panel: Photograph of Eppley PIRs, left, stock Eppley PIR; right, IMET PIR.

of the calibration and place more of the contribution to the long-wave measurement from term (I), which has no calibration coefficient.

Finally, removing the thermopile removed the necessity of high gain amplification as well. This circuit has proved susceptible to R/F interference. Using the thermistors requires just a simple resistance bridge, which is easy to design, is stable, and requires low power. The associated electronics will be much simpler and robust.

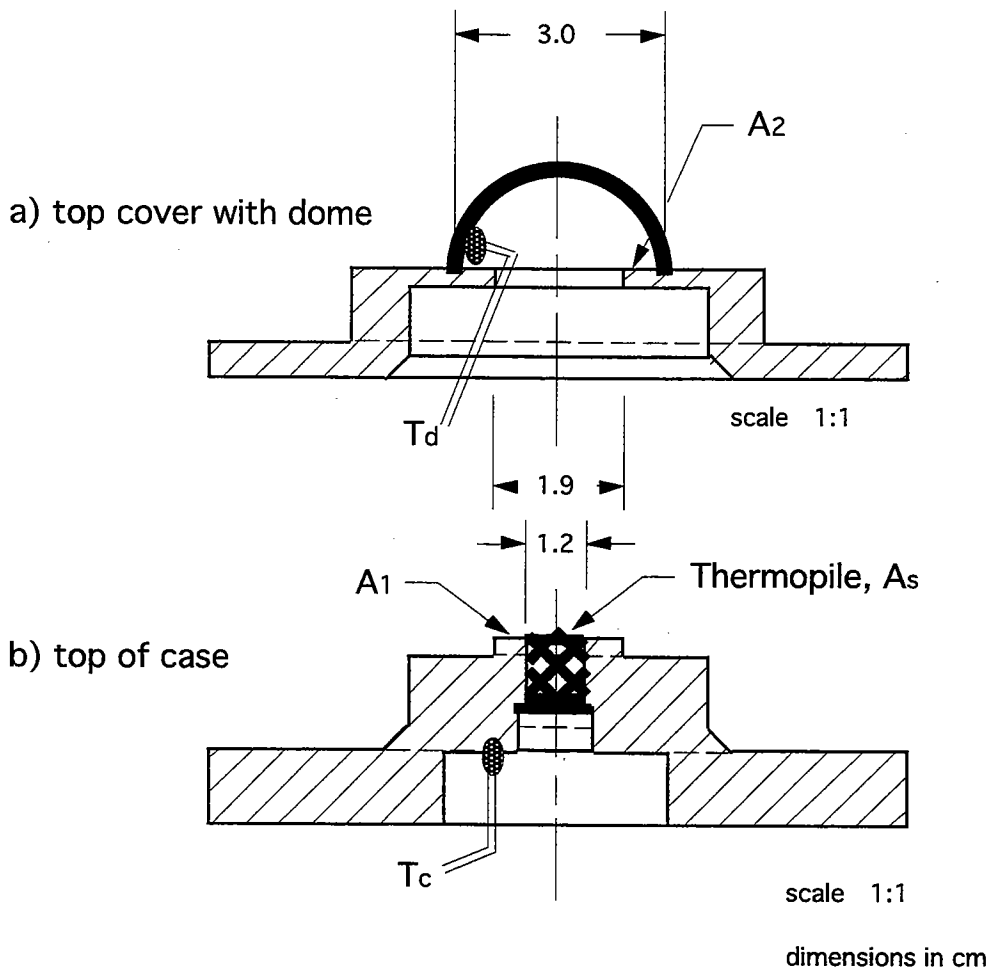
### 3.2 The dome heating correction

Reconsider the dome heating, term (III). In the Albrecht and Cox (1977) formulation, their  $k$  equals the  $\epsilon_d/\tau_d^{SW}$  or  $B$  in the equations. They report that  $k$  may be as large as 4.0 for a stock Eppley sensor. Olivieri (1991) also suggests that this coefficient is about 4.0. Due to the restraint that  $\epsilon_d + \tau_d + \rho_d = 1$ , it is not possible to reach a coefficient of 4.0 using either of the suggested values by Dickey et al. (1994) or Olivieri for long-wave emittance.

In the above formulation it has been assumed that the area of the thermopile surface is equal to the total area under the dome. This is not the case in the Eppley pyrgeometer (see Fig. 3). The dome is attached to a removable cover. In the IMET version, the cover is aluminum with an exterior coating of white paint. The VAWR version has a cover made of stainless steel. In both configurations, a lip of this material,  $A_2$ , is exposed to the area under the dome. The case in both sensors is made of aluminum and also has a surface,  $A_1$ , that is exposed under the dome. The true thermopile surface,  $A_s$ , is a fraction of the total area under the dome. (The geometry under the dome also includes a thermistor, which is glued to the inside of the dome. The area of the glue holding the dome and thermistor is  $A_G$ .) An accurate assessment of the heat budget on the thermopile surface would include the emittance and reflectance of all these surfaces.

For example, consider the  $B(T_c^4 - T_d^4)$  term (III). Taking the long-wave emittance from the additional surfaces,  $\epsilon_1$ ,  $\epsilon_2$ , and  $\epsilon_G$ , and assume the surface temperatures on  $A_1$ ,  $A_2$ , and  $A_G$  are equal to  $T_d$ . Using a direct and reflected path for the emitted radiation, the coefficient becomes

$$\frac{\epsilon_d}{\tau_d} + \frac{(1 + \rho_d)(\epsilon_1 A_1 + \epsilon_2 A_2 + \epsilon_G A_G)}{\tau_d(A_1 + A_2 + A_s)} \quad (20)$$



c) schematic of area under dome

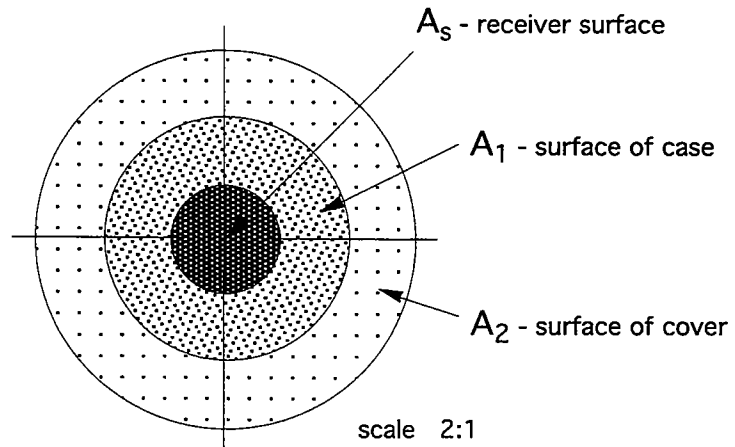


Figure 3: Schematic of stock Eppley PIR.

This formulation allows for larger possible values of  $B$ . Taking the emissivities as

$$\begin{aligned}\epsilon_{\text{stainless}} &= 0.6 \text{ (slightly oxidized)} \\ \epsilon_{\text{aluminum}} &= 0.1 \\ \epsilon_{\text{glue}} &= 0.9\end{aligned}$$

the normalized areas

$$A_{\text{Total}} = A_1 + A_2 + A_s ; \quad a_1 = A_1/A_{\text{Total}} = 0.242 ; \quad a_2 = 0.6 ; \quad a_G = 0.1$$

and the values suggested by Dickey et al. lead to the estimates

$$B = 3.6 \text{ for stock Eppley (VAWR) and } B = 2.0 \text{ for IMET .}$$

Thus, the different materials used in the case will lead to large differences in the sensitivity to the dome temperature. The IMET PIR is made of aluminum and should be less sensitive to temperature differences between the dome and the case than the stock Eppley PIR. The constant  $B$  has been estimated by Dickey et al. for four different IMET sensors. The individual values range from about 1.4 to 2.2. Fairall et al. (1998) show a table of values of  $B$  from all of our calibrations of IMET PIRs. The range of values of 3.2 to 4.4 is consistent with the above calculations.

A simple experiment was conducted to test the hypothesis that the cover material and geometry has a significant effect on the heat budget estimation on the thermopile surface. An Eppley PIR [S/N 27185; 4.19 mv/(W m<sup>-2</sup>)], an IMET PIR [S/N 27926; 4.19 mv/(W m<sup>-2</sup>)], and an Eppley 8-48 short-wave sensor were placed side by side in a shaded room. Both PIRs were equipped with the internal circuit and no dome temperature measurements were made. The long-wave sensors were allowed to reach equilibrium and yielded the same estimates of  $LW \downarrow$ . The shade was removed, allowing a direct path for the solar insolation for 140 seconds, then the shade was replaced. Two typical runs are shown in Figure 4. Eppley specifications give a response time of 2 seconds. The response observed has two time scales. The first is the rapid response of the thermopile reacting to the additional long-wave radiation. The response is short (4–8 seconds) because the mass of the thermopile is small. After the initial rapid rise, the output continues to rise for the duration of the solar insolation. The VAWR

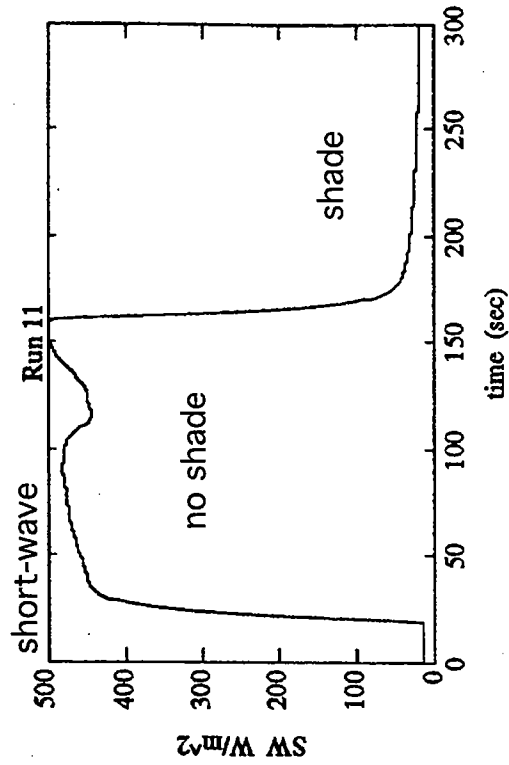
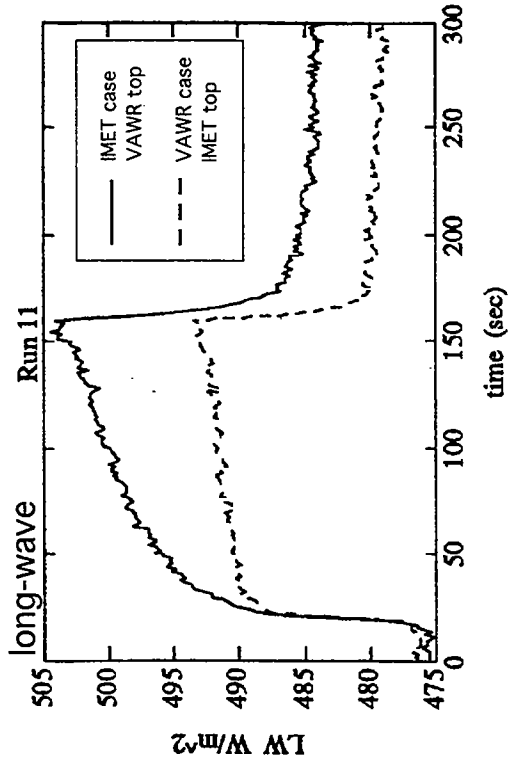
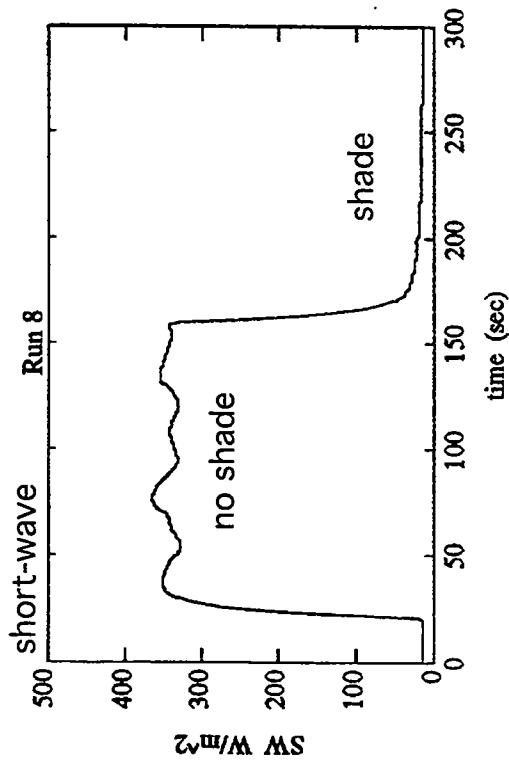
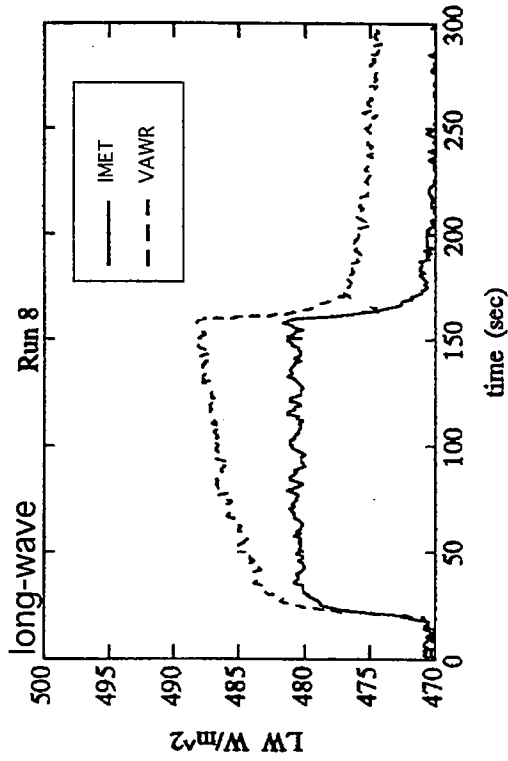


Figure 4: Example of radiative heating in stock IMET and VAWR type PIRs. In Run 8, an IMET and a VAWR PIR, along with a pyrgeometer, were exposed to sunlight for 140 sec then covered. Note rapid initial response of the long-wave as the thermopile responds, then the gradual increase as the dome and cover begin to heat up. The VAWR has a much larger error at the end of 140 sec. In Run 11, the covers from the VAWR and IMET were switched. The larger error is found to track with the VAWR cover, not with the case.



output, however, rises much faster, climbing to  $7 \text{ W m}^{-2}$  above the IMET output at the end of the solar insolation. When the solar insolation is removed, the outputs drop rapidly again and quickly reach a value that is larger than the initial output by the amount equal to the increase from the slow response over the time of insolation. This same pattern was observed even if the sensor positions were switched or various shields were placed over the sensor cases leaving only the domes exposed.

The next step was to switch the covers and domes from the sensors so that the IMET had the stainless top from the VAWR and vice versa. Then the experiment was repeated. The same pattern was observed on various conditions except this time the output from the IMET rose above that of the VAWR. The excessive output due to insolation followed the cover, not the sensor. If there were a pin hole in one of the domes or the short-wave transmissivity were different between the domes, the initial response between the two instruments would be of different magnitudes. This is because the thermopile temperature will respond quickly to the increase in infrared radiation. There is a small difference ( $2\text{--}3 \text{ W m}^{-2}$ ) between the two covers just after the initial rise in the output (10 seconds after the start of insolation). The longer time scale response must be related to heating of the cover and the dome that slowly increases the radiation incident on the thermopile surface. This is not a rigorous experiment and should be redone measuring the individual thermistors and thermopile outputs separately. However, it is clear that the dome heating term tracks with the PIR dome and top and not the thermopile and case.

The effect of dome heating on the receiver can be reduced by increasing the area of the receiving surface under the dome. Like reducing the conductive heat loss term, reducing the dome heating term will lessen the dependence of measurements on calibration, putting more of the dependence on term (I), the black body radiance term, which is independent of calibration. Expanding the receiver area is easily addressed in the redesign that removes the thermopile.

## 4 Demonstration of concept

In this section we describe our efforts to build a prototype pyrgeometer based on the ideas described in the previous section. The prototype was built to be easily modified so we

could make changes in the lab to explore the thermal characteristics and responses. The instrument was not designed for field deployment but rather as a proof of concept. However, we did deploy the prototype alongside an IMET PIR on the roof of the Clark Laboratory for two weeks. From this deployment we do successfully demonstrate that the prototype not only works but performs remarkably well. This effort has proved the concept of removing the thermopile completely. The next step would be to develop the instrument for long term deployment.

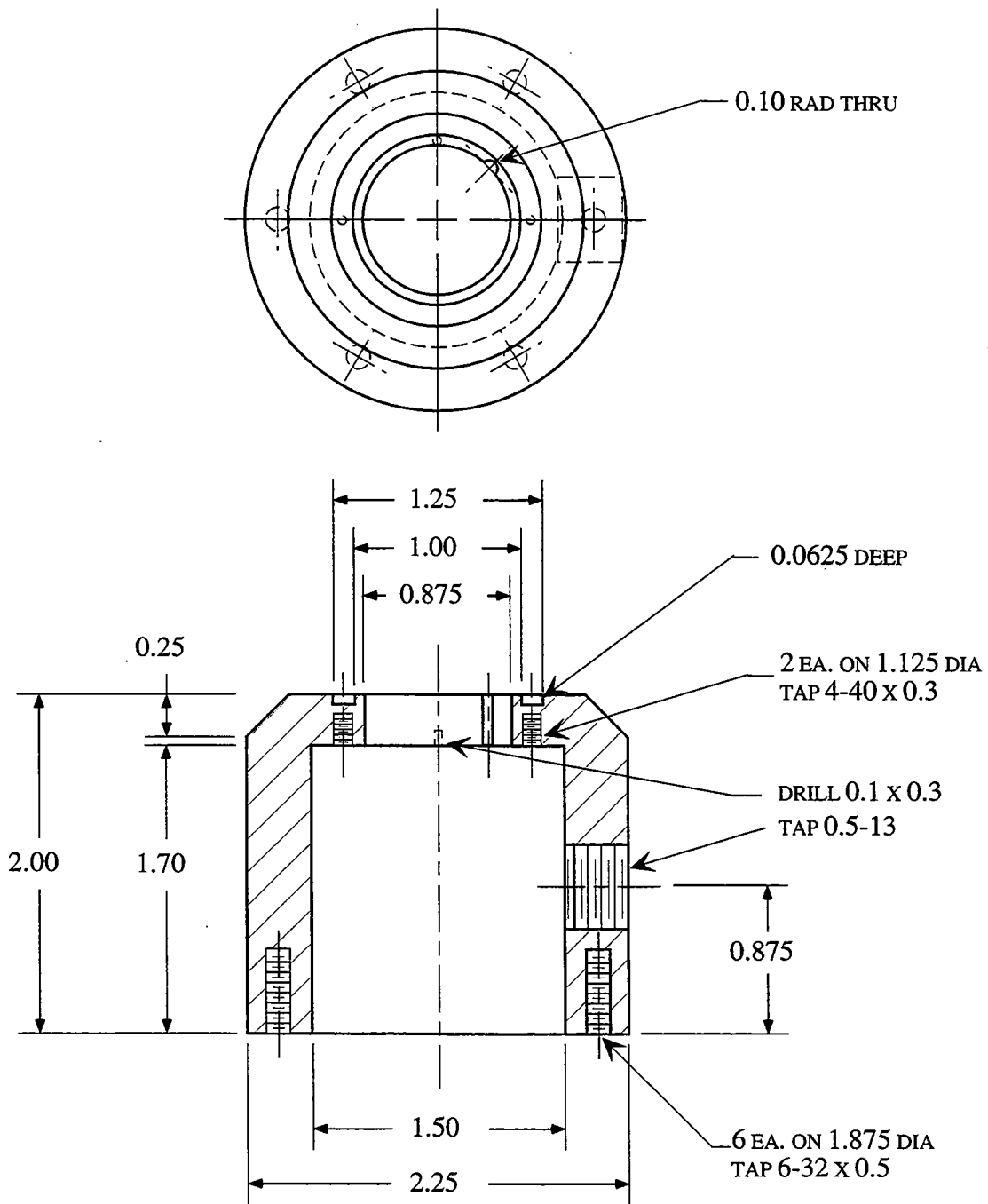
## 4.1 The prototype

A drawing of the prototype designed and built is shown in Figure 5. The body is made of aluminum and is painted with a bright white paint. The receiver surface is aluminum, 0.11 mm thick, painted with Parson's optical black lacquer. Its diameter is 2.00 cm as compared with the diameter of the dome base, 2.67 cm. Attached with thermal conducting epoxy to the middle of the underside is a 0.36 mm-diameter thermistor. The receiver disk is cemented to the tops of three 2-56 threaded rods, located near its perimeter, which project 8.4 mm above an aluminum plug insert. This insert is screwed into the inside of the body. The stainless steel rods provide a convenient low thermal conductance mounting for the receiver disk. A thermistor is potted into the body and another is potted into the receiver mounting plug insert at the base of one of the receiver support rods. The silicon dome was purchased from Eppley and is identical to the domes used in the Eppley PIR.

## 4.2 Calibration

The prototype pyrgeometer was calibrated using the same technique and equipment we use for the PIR (Payne and Anderson, 1999). Six runs are made, each one lasting 12 minutes. In three of them, data are recorded for 1 minute while the PIR is in equilibrium at room temperature, for 1 minute while the PIR is suspended upside down over water at 50°C, and for 10 minutes while the PIR is mounted in a cold black body cavity at, successively, 0.1, 5, and 10°C. In the other three runs, data are recorded for 1 minute at room temperature, for 1 minute while it is suspended over ice, and for 10 minutes while the PIR is mounted in a warm black body cavity at, successively, 30, 40, and 50°C. There is at least 1 hour between

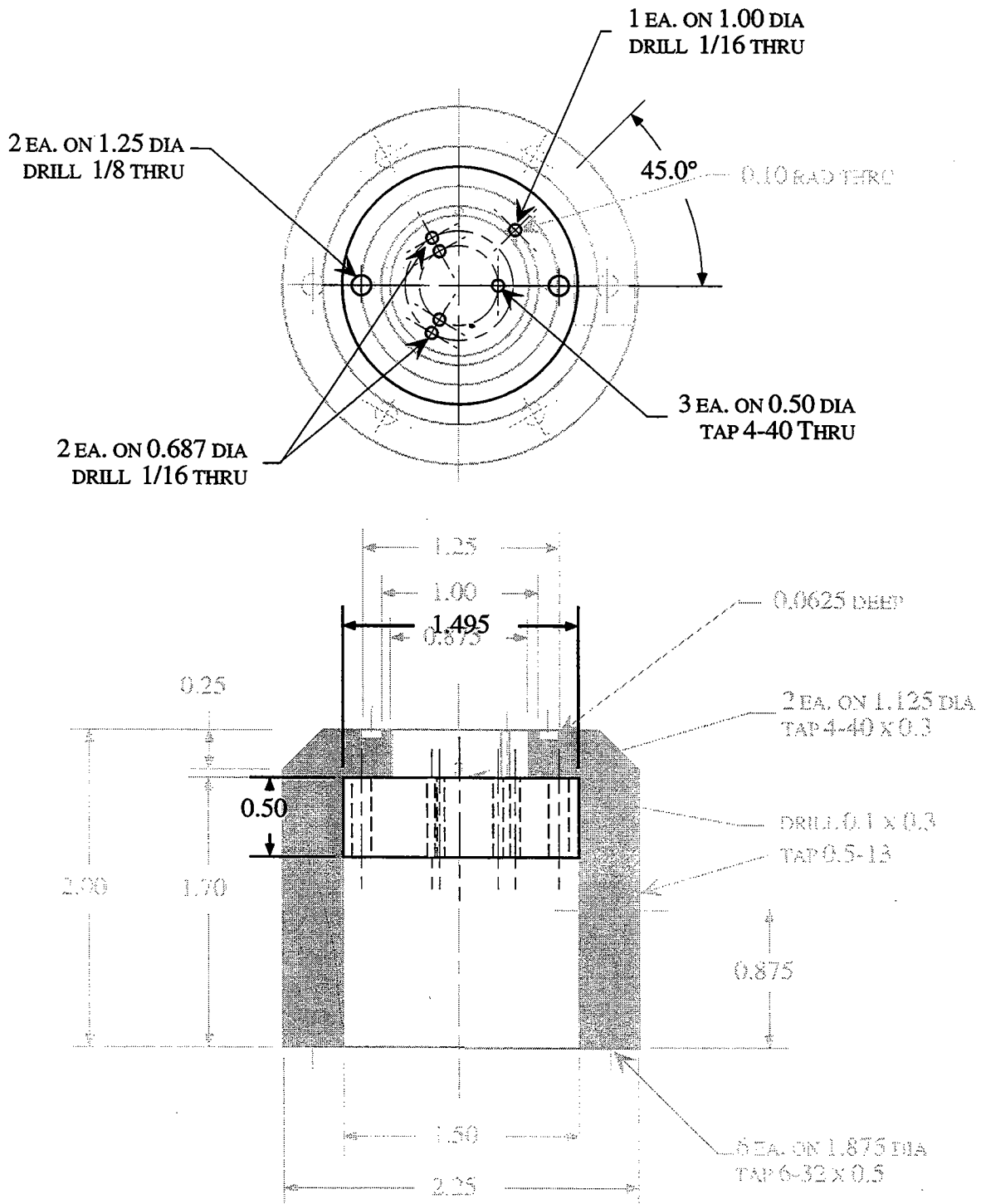
Figure 5: Drawing of pyrgeometer prototype: (a) case.



NOTE: DIMENSIONS GIVEN IN INCHES

TITLE GREEN TECHNOLOGY PROTOTYPE IMPROVED PIR	UPPER OCEAN PROCESSES WOODS HOLE OCEANOGRAPHIC INSITUTION	
	DRAWN BY STEVE ANDERSON	
SHEET 1 OF 3	DATE MAY 19, 1998	VER. 1.0

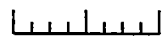
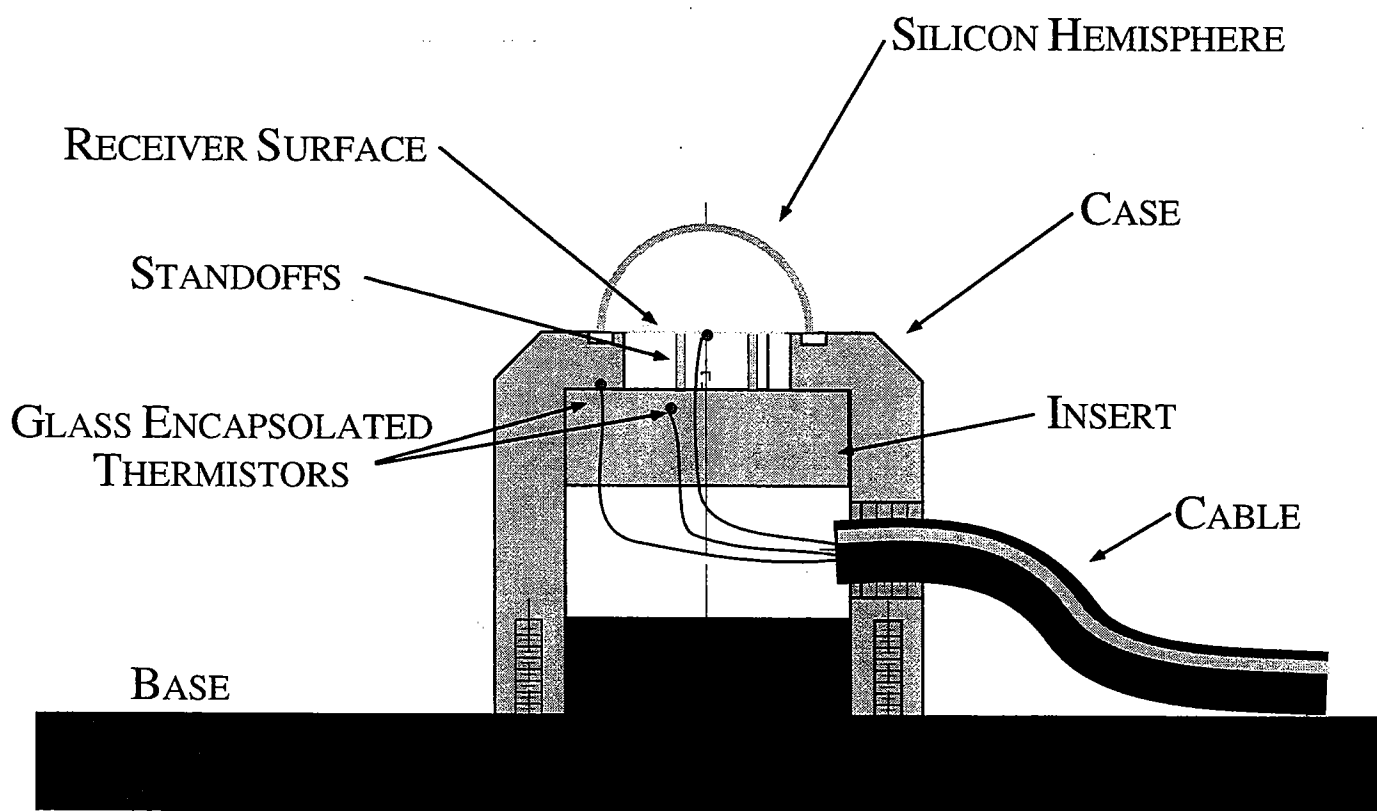
Figure 5: Drawing of pyrgometer prototype: (b) insert.



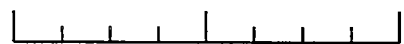
NOTE: DIMENSIONS GIVEN IN INCHES.

TITLE GREEN TECHNOLOGY PROTOTYPE IMPROVED PIR INSERT AND RECEIVER	UPPER OCEAN PROCESSES WOODS HOLE OCEANOGRAPHIC INSTITUTION		
	DRAWN BY STEVE ANDERSON		
SHEET 2 OF 3	DATE MAY 19, 1998	VER. 1.0	

Figure 5: Drawing of pyrgeometer prototype: (c) overall sketch.



0 2 CM



0 1 2 INCHES

TITLE GREEN TECHNOLOGY PROTOTYPE IMPROVED PIR INSERT AND RECEIVER	UPPER OCEAN PROCESSES WOODS HOLE OCEANOGRAPHIC INSTITUTION	
	DRAWN BY STEVE ANDERSON	
SHEET 3 OF 3	DATE MAY 19, 1998	VER. 1.0

runs to allow the PIR to return to room temperature equilibrium. One of the warm-to-cold runs is shown in Fig. 6. Note the sudden rise of the plate temperature and the slower rise of the body temperature followed by a reversal when the pyrgometer is put in the black body cavity. Where the curves cross the second time,  $T_s = T_c$  and term II in Eq. 17 is zero. Equation 17 then reduces to

$$LW \downarrow = \sigma T_s + B(T_s^4 - T_d^4) \quad (21)$$

In later versions of the pyrgometer when we measure dome temperature, we will determine the  $B$  constant. Since  $LW \downarrow$  is known from the measured temperature of the black body cavity, this will yield six independent determinations of  $B$ . Knowing  $B$ , we will compute  $A$  using the full Eq. 17 and the last data record from each of the six runs. In the prototype, without the measurement of the dome temperature, we compute six values of  $A$  from the last record neglecting term III.

### 4.3 Field intercomparison

Figures 7–10 show data from an 11-day comparison of the prototype pyrgometer with two Eppley IMET-style PIRs on the roof of the Clark building, a site with a clear view of the whole sky. Short-wave radiation from an Eppley PSP is overplotted to show where that is significant. All sensor outputs were recorded on a Campbell CR7 data logger.

The three pyrgometers track very well except during daytime periods of high short-wave radiation when the lack of a dome correction in the prototype causes its values to be anomalously high. Except in these high short-wave radiation periods, the prototype agrees with the Eppley PIRs to  $10 \text{ W m}^{-2}$ .

Figure 8 shows the components and total long-wave flux as computed from Eq. 17 without the short-wave correction term. Figure 9 shows the difference between the prototype and one of the Eppley PIRs. Except for three very short periods, the differences are of order  $10 \text{ W m}^{-2}$  or less. Figure 10 is a plot of prototype-PIR difference vs total PIR long-wave flux. The large excursions are principally during periods of high short-wave flux. There is a small dependence of the difference on the magnitude of the flux.

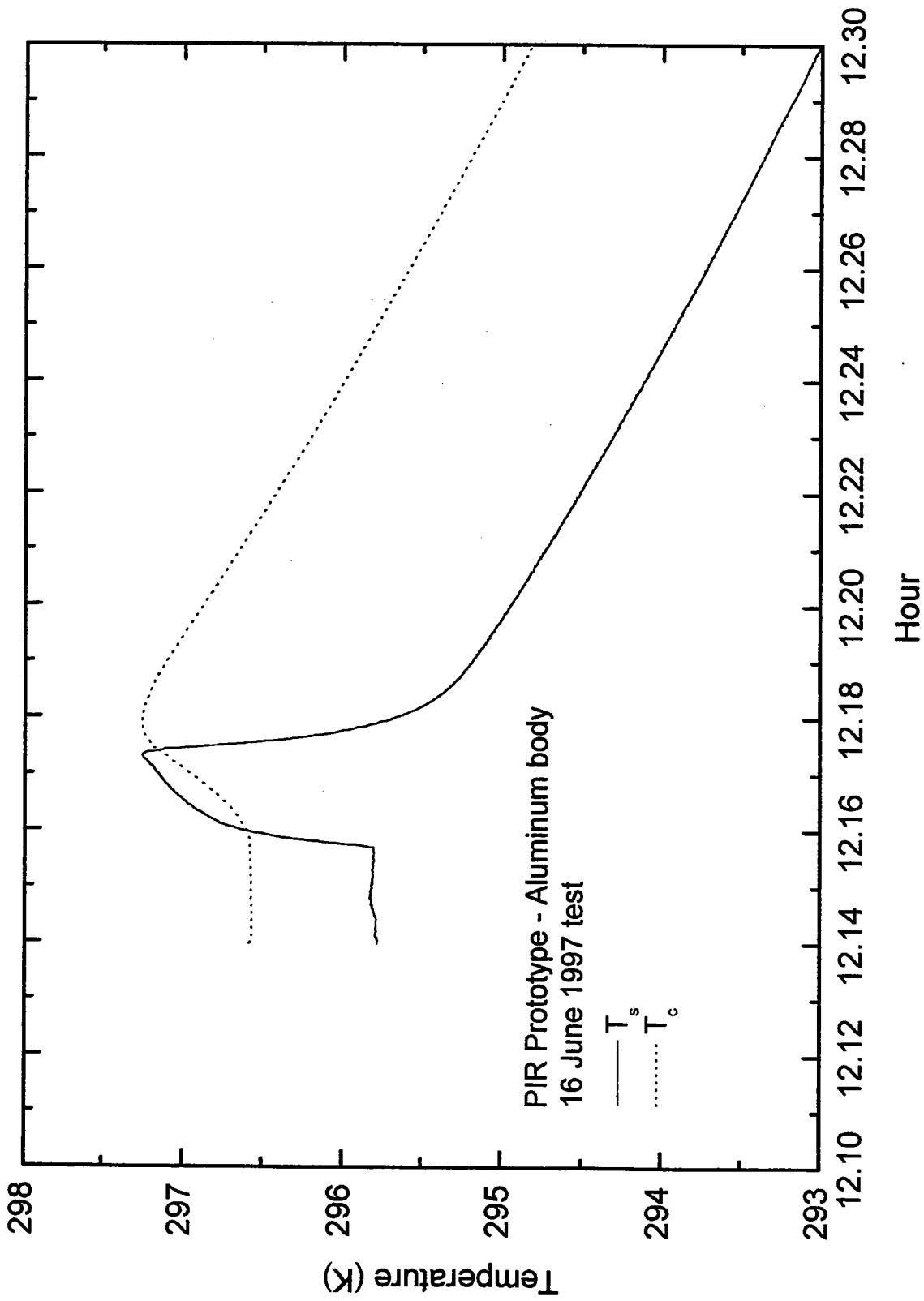


Figure 6: Calibration run: pyrometer over water at 50°C, then in black body cavity at 0.1°C.  $T_s$  and  $T_c$  are plate and body temperatures, respectively.

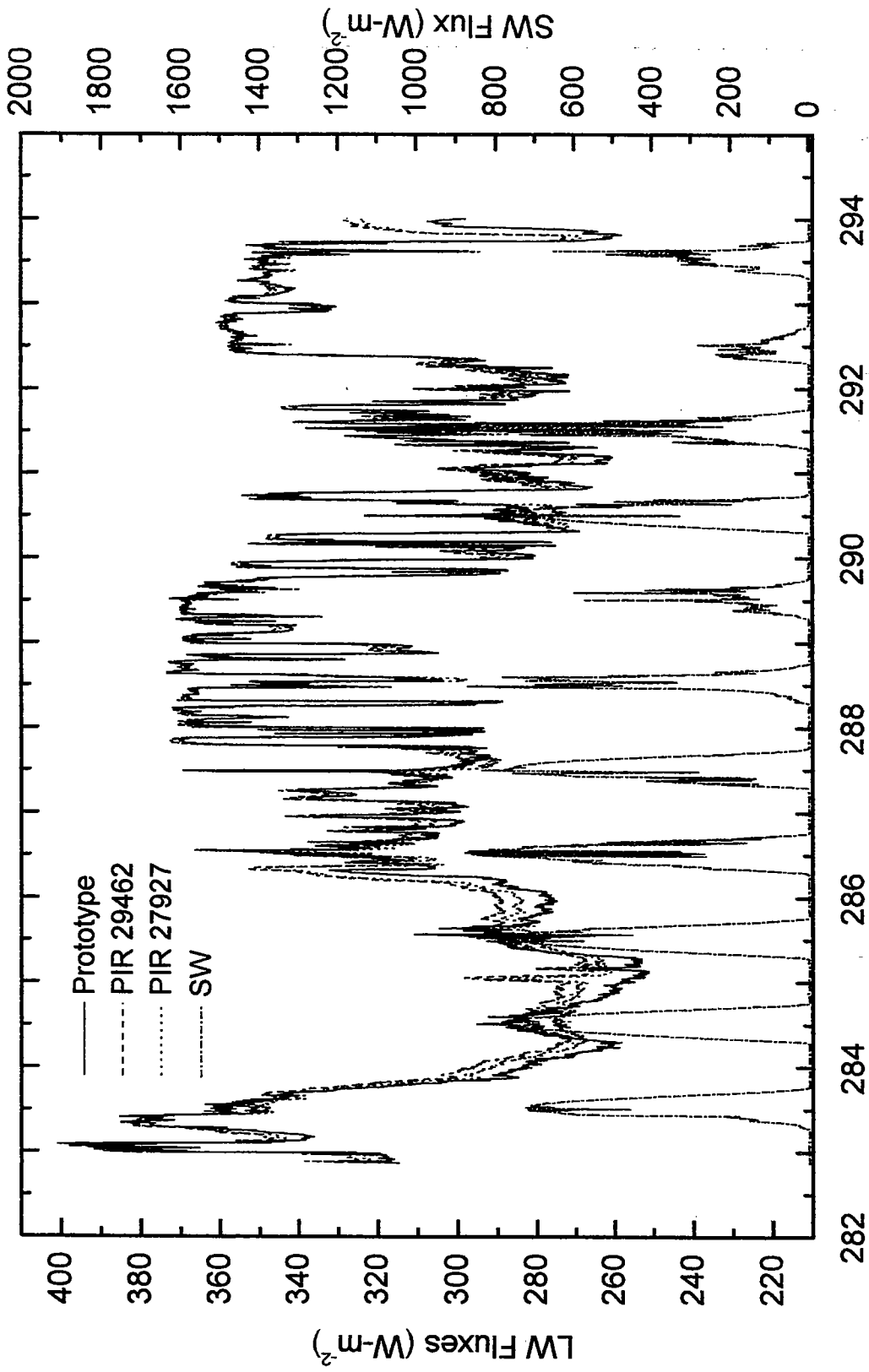


Figure 7: Total flux from two Eppley PIRs and the prototype pyrgometer in an 11-day field test vs time. Overlay of short-wave flux.



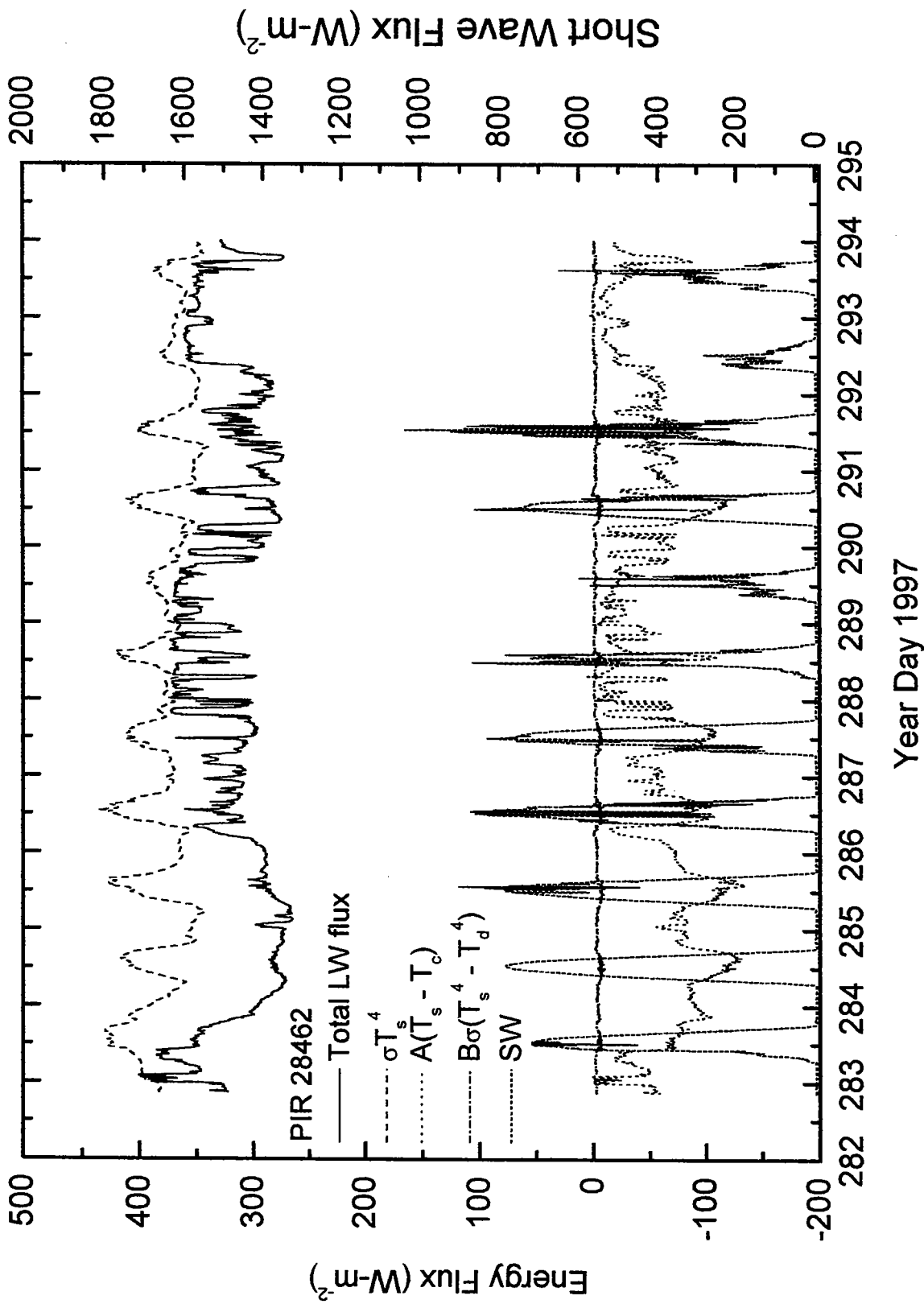


Figure 8: Components of Eppley PIR flux from Eq. 17 without short-wave correction, overlaid with short-wave flux for field test vs time.

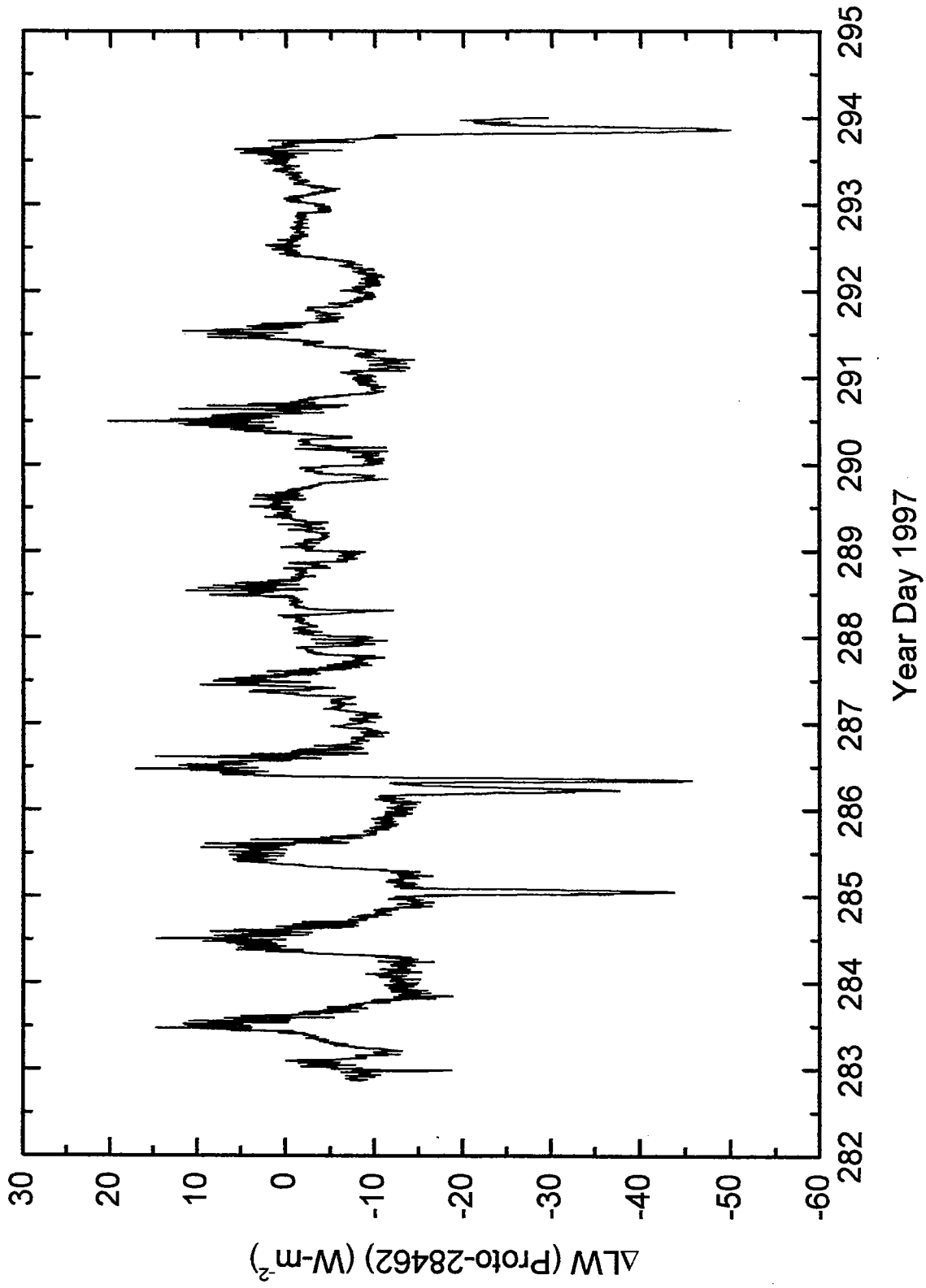


Figure 9: Plot of difference between prototype and one Eppley PIR total long-wave flux for field test vs time.

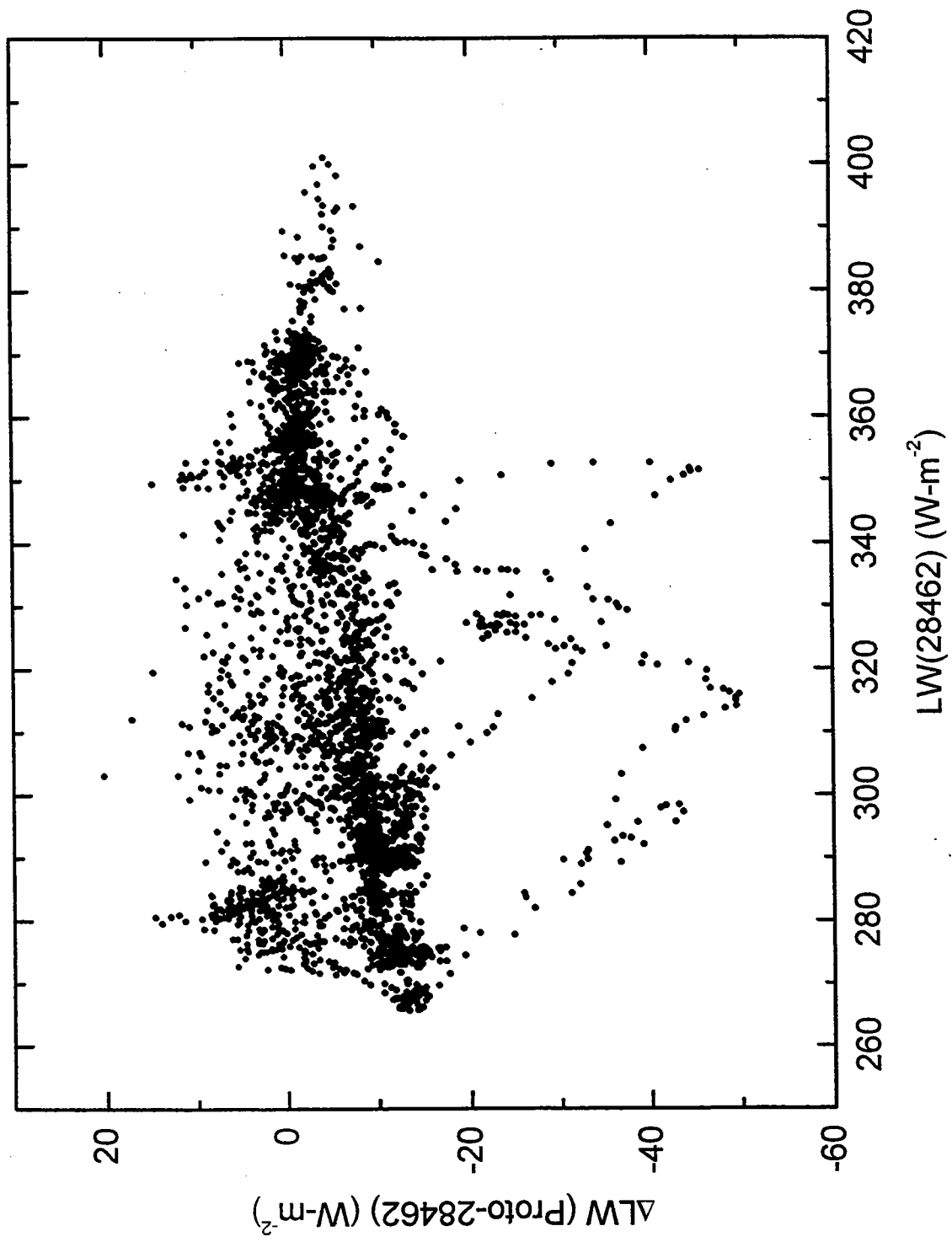


Figure 10: Plot of difference between prototype and one Eppley PIR total long-wave flux for field test vs PIR total flux.

We found it quite encouraging that the comparison showed such small differences for a prototype intended to prove the concept.

## 5 Conclusions

Our study has shown that it is possible to build a pyrgeometer to measure downwelling long-wave radiation without the use of a thermopile. The new instrument is simpler to construct and calibrate, and has a simpler theory of operation, than standard thermopile-based pyrgeometers. The comparison of data from the prototype and standard instruments demonstrates that the concept clearly works.

We have completed the first step in the development of a new meteorological instrument. The prototype pyrgeometer was able to demonstrate the concept but there still remains a lot of work before we have a field-deployable instrument capable of reliably collecting scientific-quality data in the field.

The next step is to construct a field-deployable version of the new pyrgeometer design. The prototype did not have a thermopile dome, and thus the dome heating errors could not be accounted for in the measurements. This must be included in the next version. In addition, the instrument should be rugged enough to withstand the hazards of deployment in the marine environment and functionally similar to our existing inventory of standard pyrgeometers. Once such an instrument is constructed, it should be deployed next to a standard instrument during several field experiments to gain confidence in its reliability and accuracy.

## Appendix

### Clark et al. formulation

The net long-wave radiation formula of Clark et al. (1974) is commonly used and uses the same basic parameterization as competing formulations. (Note the formula often referred to as Clark et al. is based on work by Berliand and Berliand, 1952.)

$$LW \uparrow \downarrow = \epsilon \sigma T_s^4 \left[ 0.39 - 0.05(e_a)^{1/2} \right] F(C) + 4\epsilon \sigma T_s^3 (T_s - T_a) \quad (22)$$

where the cloud cover factor is  $F(C) = (1 - bC^2)$ .  $T_s$  and  $T_a$  in the formula are given in degrees Kelvin. The vapor pressure,  $e_a$  (in mbars), is calculated using Buck's (1981) formula for saturation vapor pressure of pure water corrected for salt water which used the measured relative humidity, barometric pressure and sea surface temperature. The cloud cover parameter  $b$  is a function of latitude:

	50°N	40°N	30°N	20°N	10°N	5°N	Equator
$b$	0.73	0.69	0.64	0.60	0.56	0.53	0.51

The cloud cover,  $C$ , is the cloud cover fraction from 0.0 to 1.0 where 0.0 corresponds to a clear sky and 1.0 is overcast. The clear sky  $LW \uparrow \downarrow$  is larger than that of a cloud-covered sky with the same  $T_s$ ,  $T_a$ , and  $e_a$ .

### Cloud cover estimation

The cloud cover can be estimated from the measuring incoming short-wave radiation. Using the cloud factor formula from Kimball (1928)

$$C = 1.41 \left[ 1 - \frac{SW_{\text{obs}} \downarrow}{SW_{\text{CS}} \downarrow} \right] \quad (23)$$

where  $SW_{\text{obs}} \downarrow$  is the observed incoming solar radiation,  $SW_{\text{CS}} \downarrow$  is the theoretical clear sky value for incoming solar radiation. The  $SW_{\text{CS}} \downarrow$  is calculated using the formulae given in the Smithsonian Meteorological Tables (List, 1951):

$$\begin{aligned}
SW_{CS\downarrow} &= SW_{\text{diffuse}} + SW_{\text{direct}} \\
&= \left[ 0.5 \frac{J_0}{r^2} (0.91 - a^{\csc \alpha}) \sin \alpha \right] + \left[ \frac{J_0}{r^2} a^{\csc \alpha} \sin \alpha \right] \\
&= 0.5 \frac{J_0}{r^2} (0.91 - a^{\csc \alpha}) \sin \alpha
\end{aligned} \tag{24}$$

where  $J_0$  is the solar constant,  $\alpha$  is the sun's inclination,  $r$  is the radius vector of the earth, and  $a$  is the atmospheric transmission coefficient (ATC). The values of  $z$  and  $r$  are determined by calculating the local solar time and using the formula found in "The Astronomical Almanac, 1986," US Naval Observatory, page C24. (Also see "Almanac for Computers 1988," Nautical Almanac Office, US Naval Observatory.) The atmospheric transmission coefficient must be estimated using the  $SW_{\text{obs}\downarrow}$  during times of clear sky.

$$a = \left[ \frac{2SW_{\text{obs}\downarrow} r^2}{J_0 \sin \alpha} - 0.91 \right]^{\sin \alpha} \tag{25}$$

The ATC is a function of the sun's zenith but is modeled here as a constant for all angles. Thus, values estimated at dawn and dusk will be different than those estimated at noon.

There are many pitfalls in using the  $SW_{\text{obs}\downarrow}$  to estimate the cloud cover. When the sun is near the horizon, a cloud far away from the observation site may block the solar insolation yielding a high cloud-cover estimate even if there are no overhead clouds. The opposite may also occur when clear sky near the horizon leaves a direct path for the solar insolation but the overhead sky is nearly completely cloud-covered. Thus the cloud-cover formulation of Kimball (1928) is not expected to yield accurate cloud-cover estimates on a minute-to-minute (or even hour-to-hour) time scale. Another difficulty is that the cloud cover can only be estimated during daylight hours. The best that can be hoped for is that the estimated cloud cover averaged over the daylight hours will reflect a daily average cloud cover.

## **Acknowledgments**

Mark St. Pierre provided mechanical shop support services. Eppley Laboratories, Inc. of Newport, Rhode Island, manufactured the silicon domes for the prototype instrument. This development project was funded by the Cecil H. and Ida M. Green Technology Innovation Fund. Additional funding to develop a field-deployable version of the instrument was provided by the National Science Foundation Grant OCE98-18470.

## References

- Alados-Arboledas, L., J. Vida, and J. I. Jimenez, 1988: Effects of solar radiation on the performance of pyrgeometers with silicon domes. *Journal of Atmospheric and Oceanic Technology*, **5**, 666–670.
- Albrecht, B., and S. K. Cox, 1977: Procedures for improving pyrgeometer performance. *Journal of Applied Meteorology*, **16**, 188–197.
- Berliand, M. E., and T. G. Berliand, 1952: Measurement of the effective radiation of the earth with varying cloud amounts. *Izvestiya Akademii Nauk SSSR, Seriya Geofizicheskaya*, No. 1.
- Buck, A. L., 1981: New equations for computing vapor pressure and enhancement factor. *Journal of Applied Meteorology*, **20**, 1527–1532.
- Clark, N. E., L. Eber, R. M. Laurs, J. A. Renner, and J. F. T. Saur, 1974: Heat exchange between ocean and atmosphere in the eastern North Pacific for 1961–1971. NOAA Technical Report NMFS SSRF-682, U.S. Dept. of Commerce, Washington, D.C., 103 pp.
- Dickey, T. D., D. V. Manov, R. A. Weller, and D. A. Siegel, 1994: Determination of longwave heat flux at the air–sea interface using measurements from buoy platforms. *Journal of Atmospheric and Oceanic Technology*, **11**, 1057–1078.
- Fairall, C. W., P. O. G. Persson, E. F. Bradley, R. E. Payne, and S. P. Anderson, 1998: A new look at calibration and use of Eppley Precision Infrared Radiometers. Part I: Theory and application. *Journal of Atmospheric and Oceanic Technology*, **15**, 1229–1242.
- Foot, J. S., 1986: A new pyrgeometer. *Journal of Atmospheric and Oceanic Technology*, **3**, 363–370.
- Fung, I. Y., D. E. Harrison, and A. A. Lacis, 1984: On the variability of the net longwave radiation at the ocean surface. *Reviews of Geophysics and Space Physics*, **22**(2), 177–193.
- Kimball, H. H., 1928: Amount of solar radiation that reaches the surface of the earth on the land and on the sea and methods by which it is measured. *Monthly Weather Review*, **56**, 393.
- List, R. J., 1951: Smithsonian Meteorological Tables, Sixth Revised Edition. The Smithsonian Institution; 527 pp.



- Olivieri, J., 1991: Measurement of longwave downward irradiance using a "PIR" pyrgeometer. Appendix B in *Radiation and Climate, Second Workshop on Implementation of the Baseline Surface Radiation Network (Davos, Switzerland, 6–9 August 1991)*, International Council of Scientific Unions, World Meteorological Organization Technical Document No. 453, 26 pp.
- Payne, R. E., and S. P. Anderson, 1999: A new look at calibration and use of Eppley Precision Infrared Radiometers. Part II: Calibration and use of the Woods Hole Oceanographic Institution Improved Meteorology Precision Infrared Radiometer. *Journal of Atmospheric and Oceanic Technology*, **16**, 739–751.
- Philipona, R., C. Frohlich, and C. Betz, 1995: Characterization of pyrgeometers and the accuracy of atmospheric long-wave radiation measurements. *Applied Optics*, **34**, 1598–1605.



## DOCUMENT LIBRARY

*Distribution List for Technical Report Exchange – July 1998*

University of California, San Diego  
SIO Library 0175C  
9500 Gilman Drive  
La Jolla, CA 92093-0175

Hancock Library of Biology & Oceanography  
Alan Hancock Laboratory  
University of Southern California  
University Park  
Los Angeles, CA 90089-0371

Gifts & Exchanges  
Library  
Bedford Institute of Oceanography  
P.O. Box 1006  
Dartmouth, NS, B2Y 4A2, CANADA

NOAA/EDIS Miami Library Center  
4301 Rickenbacker Causeway  
Miami, FL 33149

Research Library  
U.S. Army Corps of Engineers  
Waterways Experiment Station  
3909 Halls Ferry Road  
Vicksburg, MS 39180-6199

Marine Resources Information Center  
Building E38-320  
MIT  
Cambridge, MA 02139

Library  
Lamont-Doherty Geological Observatory  
Columbia University  
Palisades, NY 10964

Library  
Serials Department  
Oregon State University  
Corvallis, OR 97331

Pell Marine Science Library  
University of Rhode Island  
Narragansett Bay Campus  
Narragansett, RI 02882

Working Collection  
Texas A&M University  
Dept. of Oceanography  
College Station, TX 77843

Fisheries-Oceanography Library  
151 Oceanography Teaching Bldg.  
University of Washington  
Seattle, WA 98195

Library  
R.S.M.A.S.  
University of Miami  
4600 Rickenbacker Causeway  
Miami, FL 33149

Maury Oceanographic Library  
Naval Oceanographic Office  
Building 1003 South  
1002 Balch Blvd.  
Stennis Space Center, MS, 39522-5001

Library  
Institute of Ocean Sciences  
P.O. Box 6000  
Sidney, B.C. V8L 4B2  
CANADA

National Oceanographic Library  
Southampton Oceanography Centre  
European Way  
Southampton SO14 3ZH  
UK

The Librarian  
CSIRO Marine Laboratories  
G.P.O. Box 1538  
Hobart, Tasmania  
AUSTRALIA 7001

Library  
Proudman Oceanographic Laboratory  
Bidston Observatory  
Birkenhead  
Merseyside L43 7 RA  
UNITED KINGDOM

IFREMER  
Centre de Brest  
Service Documentation - Publications  
BP 70 29280 PLOUZANE  
FRANCE



<b>REPORT DOCUMENTATION PAGE</b>	1. REPORT NO. <b>WHOI-00-13</b>	2.	3. Recipient's Accession No.
4. Title and Subtitle <b>An Improved Long-Wave Radiometer</b>		5. Report Date <b>December 2000</b>	
7. Author(s) <b>Steven P. Anderson</b> <b>and</b>		8. Performing Organization Rept. No. <b>WHOI-00-13</b>	
9. Performing Organization Name and Address  <b>Woods Hole Oceanographic Institution</b> <b>Woods Hole, Massachusetts 02543</b>		10. Project/Task/Work Unit No.  11. Contract(C) or Grant(G) No. <b>(C) 8184700</b> <b>(G)</b>	
12. Sponsoring Organization Name and Address  <b>Cecil H. and Ida M. Green Technology Innovation Awards Program</b> <b>National Science Foundation</b>		13. Type of Report & Period Covered <b>Technical Report</b>  14.	
15. Supplementary Notes <b>This report should be cited as: Woods Hole Oceanog. Inst. Tech. Rept., WHOI-00-13.</b>			
16. Abstract (Limit: 200 words)  This report describes the development of an improved long-wave radiometer (pyrgeometer) for deployment on ships and buoys. Standard pyrgeometers use a thermopile to measure the temperature gradient between the receiver surface and the instrument case, and thus infer the receiver temperature and incident radiation. The key design change employed in the new radiometer is to remove the thermopile and replace it with a small, glass-encapsulated thermistor to measure the receiver temperature directly. To prove the concept, a prototype radiometer was built and calibrated. It was then deployed outside for a period of a week on the roof of the Clark Laboratory (Quissett Campus, Woods Hole Oceanographic Institution) to demonstrate the feasibility of the new concept. Data from the prototype were compared to those from a pair of standard radiometers. The intercomparison shows that the prototype performed surprisingly well. It was able to capture all the variability observed by the standards with only a small bias. The next step in the design process, which has been funded by the National Science Foundation, is to build a rugged version of the prototype that can be deployed in the field.			
17. Document Analysis    a. Descriptors <b>Long-Wave Radiometer</b> <b>Meteorological Sensor</b> <b>Thermistors</b>  b. Identifiers/Open-Ended Terms    c. COSATI Field/Group			
18. Availability Statement  <b>Approved for public release; distribution unlimited.</b>		19. Security Class (This Report) <b>UNCLASSIFIED</b>	21. No. of Pages <b>43</b>
		20. Security Class (This Page)	22. Price

